

Acoustic detection of microbubble resonance

D. H. Thomas,^{1,a)} P. Looney,¹ R. Steel,¹ N. Pelekasis,² W. N. McDicken,¹ T. Anderson,¹ and V. Sboros¹

¹Medical Physics, The University of Edinburgh, Edinburgh EH16 4SB, United Kingdom

²Department of Mechanical Engineering, University of Thessaly, Volos 38834, Greece

(Received 23 December 2008; accepted 15 May 2009; published online 16 June 2009)

Large numbers of acoustic signals from single lipid-shelled Definity® microbubbles have been measured using a calibrated microacoustic system and a two population response observed. Theoretical results based on the Mooney–Rivlin strain softening shell model have been used to identify these populations as primary resonant and off-primary resonant scatter. An experimentally measured size distribution was used to provide the initial resting radius for the simulations, and the responses agree well with the experimental data. In this way, the primary resonant or off-primary resonant behavior of a microbubble can be studied, with potential benefits to both signal processing techniques and microbubble manufacture. © 2009 American Institute of Physics.

[DOI: 10.1063/1.3151818]

When an acoustic pressure wave is incident upon a gas bubble immersed in a liquid, the incident acoustic energy causes the encapsulated gas to vibrate, producing acoustic emission containing distinct harmonics of the excitation frequency. This is the basis of using encapsulated microbubbles (MBs) to improve the contrast in ultrasonic images of microvasculature in various diagnostic techniques. The scattered signal is at a maximum when the bubble in question is driven at its primary resonance frequency which is dependent upon, among others, the shell parameters, incident pulse characteristics, and initial bubble radius.¹

Single MB signals (Definity®, Lantheus Medical Imaging, N Belarica, MA) have been measured experimentally using a commercial ultrasound imaging system, with a fully characterized transmitter and receiver.² A flow tank with hydrodynamic focusing was used to direct a submillimeter-wide stream of individual microbubbles along the axis of the ultrasonic beam.^{3,4} Figure 1 shows examples of the two types of response measured experimentally in response to a 1.6 MHz 550 kPa peak negative pressure (PNP) six cycle pulse.

A typical low amplitude signal, Fig. 1(a), is strongly harmonic (ratio of fundamental to second harmonic energy densities equals 0.65) and has a similar envelope of scatter as the transmit pulse (omitted here to save space). The envelope of the signal was detected using a quadrature amplitude demodulation method implemented in MATLAB (R2007b, Mathworks). A typical high amplitude signal, Fig. 1(c), has an increased fundamental component of scatter (fundamental to harmonic ratio of 3.97) and shows an increasing amplitude of scatter with time. Maximum fundamental amplitude response defines primary resonance. The increasing envelope of scatter at increased amplitudes has previously been identified as a characteristic of forced damped simple harmonic oscillators driven at resonance.⁵

Figure 2 displays the two population distribution of scatter from 235 single MBs exposed to the same incident pulse. A normalized cross correlation technique was used to compare the envelope of signals from different MBs and confirmed that the increasing envelope was a significant characteristic for the primary resonant population of Fig. 2. When

compared to a “reference” MB signal, Fig. 1(a), of constant amplitude (similar to the incident pulse), a signal with increasing amplitude over time has a decreased peak normalized cross correlation than one with similar constant amplitude. Visual inspection of all the MB signals recorded confirms that only these two types of envelopes were detected. An arbitrary threshold of 0.7 peak normalized cross correlation may be used to efficiently separate the scatter into two populations, as shown in Fig. 2. Although this technique does not use a precise description of the envelope to characterize each signal, the results agree well with a cluster analysis method applied to the data, which uses a dissimilarity matrix to separate populations based upon differences in energy density alone.⁶ Figure 2 shows that normalized cross correlation selects 52 bubbles to have this characteristic resonance shape, compared to the 44 using cluster analysis. As can be seen in Fig. 2, the apparent miscategorization occurs for an insignificant number of events (below 4%). Although the above figures cannot support further statistical analysis, it is important to note that dispersities in shell and structure have been previously observed for other MBs.³ In addition, fast camera observations show motion discrepancies for lipid

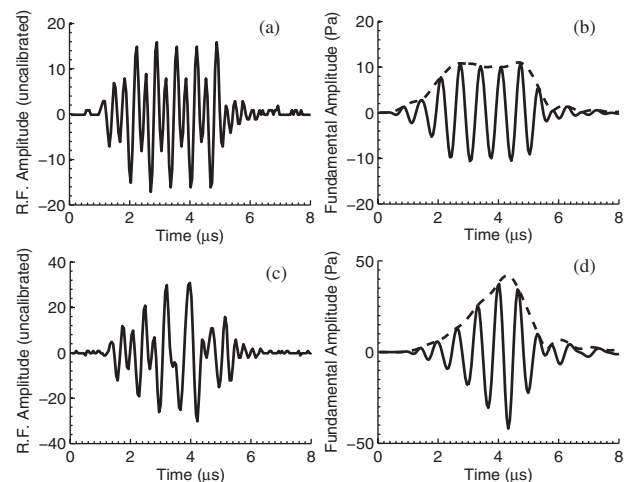


FIG. 1. Experimentally measured Definity® signals, showing two types of scatter are present within a single sample of MBs. Figures 1(a) and 1(c) show uncalibrated rf signals, and Figs. 1(b) and 1(d) show the calibrated filtered fundamental components of scatter.

^{a)}Electronic mail: d.h.thomas@ed.ac.uk.

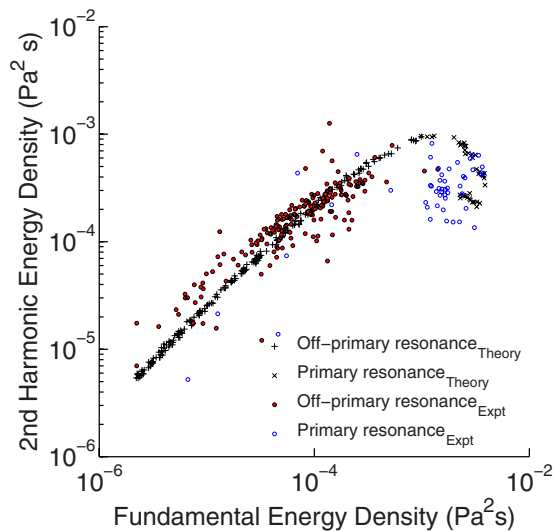


FIG. 2. (Color online) Experimental and theoretical signals from 235 single bubbles, in response to a 1.6 MHz, 550 kPa PNP six cycle pulse. Signals have been decomposed into fundamental and 2nd harmonic scatter, and classified as primary resonant or off-primary resonant scatter, using a normalized cross-correlation method. The experimental data shows good agreement with the theoretical signals (24% of scatterers defined to be at primary resonance).

MBs of the same size.⁷⁻⁹ The primary resonant scatterers (22% of the total) produce the majority of the total fundamental energy of scatter from a distribution of bubbles (70% of the fundamental, 15% of the second harmonic, and 51% of the third harmonic energy of scatter). The rest of the scatter is provided by the off-primary resonance signals.

The equations of motion for the liquid, derived from the conservation equations for mass and momentum, allow ordinary differential equations to be derived for the bubble radius as a function of time. In this way, the forced oscillations of the encapsulated bubbles can be predicted and the subsequently emitted pressure waves analyzed in comparison with experimental results, providing further understanding of the above observations.

The Keller–Miksis equation¹⁰ models the surrounding liquid by assuming linear compressibility and has the advantage over the Rayleigh–Plesset model in accounting for radiation damping. This provides improved MB motion calculation for acoustic pressures that are applicable in diagnostic ultrasound imaging.¹¹ The soft phospholipid shell of Definity® has been assumed to behave as a strain-softening material, as defined by the Mooney–Rivlin model.¹² The main parameters used in the shelled models to describe the behavior of the encapsulating lipid shell are the shell thickness (d_s), shell stiffness (G_s), and the shell viscosity (η_s).¹³ G_s and η_s have been previously estimated using ultrasound attenuation measurements.^{14,15} The values for these are here initially chosen to be $d_s=15$ nm, $G_s=50$ MPa, and $\eta_s=1$ Pa s.^{16,17} The associated ordinary differential equation has been solved for a variety of bubble radii, using a Runge–Kutta method as applied by the ODE solver “ode23” in MATLAB. The incident ultrasound pulses used for the above experiments were used here. The Vokurka equation¹⁸ was then used to calculate the scattered pressure P at a distance $r=0.075$ m (as used experimentally) from a given MB radius R_0 , providing the results shown in Fig. 3.

This shows the variations in energy of response with resting radius, as decomposed into their fundamental and

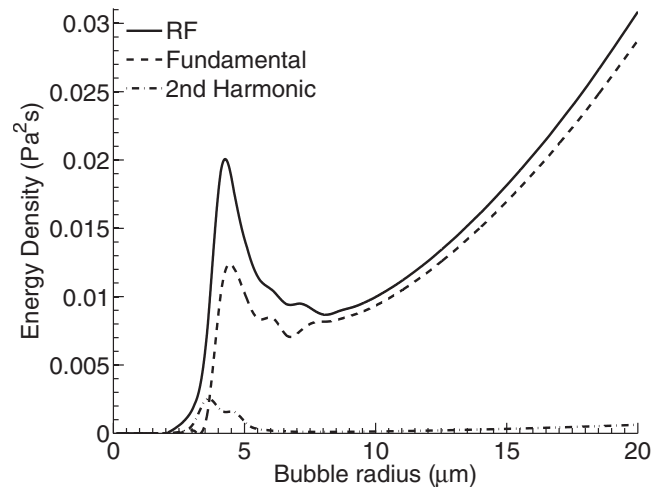


FIG. 3. Variation in energy density as predicted by the Mooney–Rivlin strain softening model, in response to an experimentally measured 1.6 MHz, 550 kPa PNP six cycle pulse.

second harmonic components (using the same elliptical filters as used in analysis of the experimental data). Primary resonance frequency (f_{res}) and the associated primary resonance radius (R_{res}) is defined as the frequency at which fundamental scatter is at a maximum¹⁹ (here $R_{\text{res}}=4.54$ μm). The amount of harmonic component in the respective bubble’s responses differs significantly from below to above primary resonance. The Mooney–Rivlin model predicts that in response to a 1.6 MHz 550 kPa PNP six cycle pulse, the peak in fundamental scatter (0.0121 Pa² s at $R=4.54$ μm) is shifted with regards to the peak in second harmonic response (0.0030 Pa² s at $R=3.72$ μm) by 0.82 μm due to higher order resonances, indicating that a maximum overall response occurs at a relatively reduced harmonic. The harmonic component is dominant up to a radius of $R_0=3.62$ μm , above which the fundamental component of scatter dominates.

The scattered pressure waves (Fig. 4) show the differences between primary and off-primary resonant scatter. Below the resonance radius, the Mooney–Rivlin model predicts a highly harmonic scatter of constant amplitude across the six cycle response [Fig. 4(a)]. As the bubble’s radius is tuned toward the primary resonance radius, the energy of scatter increases greatly, and the scatter is dominated by the fundamental components of scatter [Fig. 4(c)]. The envelope of this resonant scatter shows increasing fundamental components across the six cycle response, and the amplitude of the signal rises and falls within the insonation period producing an approximately symmetric envelope. These types of scatter match the experimental two-population observations above (Fig. 1). At large radii scatter is predominantly fundamental [Fig. 4(e)] and the envelope of scatter mimics the input pulse shape. This type of scatter has not been observed experimentally (as can be seen by the lack of large amplitude signals with low harmonic energy in Fig. 2), indicating that for the imaging parameters used here, bubbles well above resonant size are not present within the sample of Definity® MBs measured. In addition, these MBs are not of subcapillary size, which is compatible with the size distribution of Definity®.

The size distribution used for theoretical calculations was produced using a Malvern Mastersizer (Malvern Instru-

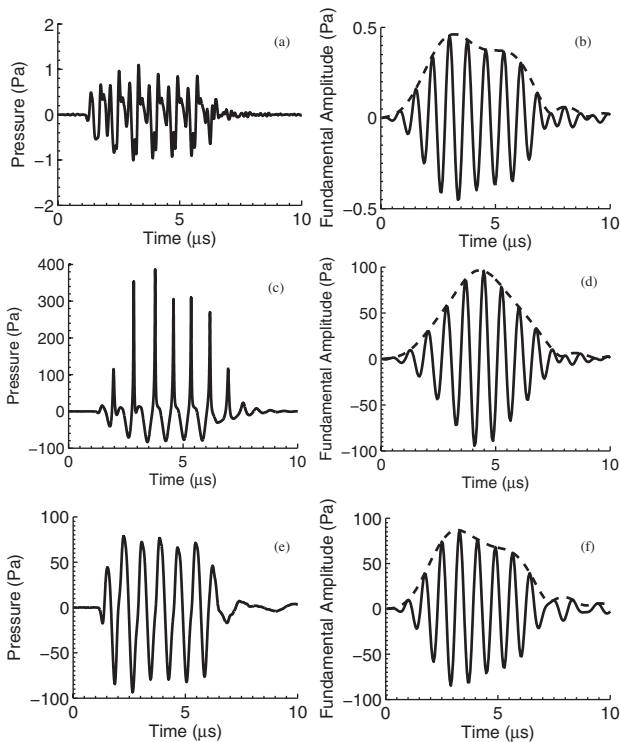


FIG. 4. Simulated variation in bubble signals for (a, b) below primary resonance ($R_0=1.60 \mu\text{m}$), (c, d) at primary resonance ($R_0=4.54 \mu\text{m}$), and (e, f) above primary resonance ($R_0=9.60 \mu\text{m}$), in response to a 1.6 MHz, 550 kPa PNP six cycle pulse. Figures 4(a), 4(c), and 4(e) show the rf scatter and Figs. 4(b), 4(d), and 4(f) show the filtered fundamental components of scatter.

ments, Worcs., U.K.), using the same experimental conditions (temperature, pressure, time since preparation, etc.) as those that produced the experimental data above. This size distribution has been used to produce a random sample of $N=235$ bubbles signals (the same number measured experimentally), whose scatter is thresholded at the noise level of the experimental system (giving a minimum initial radius of $R_0=1.9 \mu\text{m}$, in response to a 1.6 MHz 550 kPa PNP six cycle pulse), as shown in Fig. 2. Experimental error has been calculated from calibration measurements of well characterized submillimeter copper spheres² and added to the energy densities of these signals (6.2% standard error for the imaging parameters used here). Figure 2 shows the experimental and theoretical signals, demonstrating excellent agreement between the two data sets.

Note that the initial shell stiffness estimate of $G_s=50 \text{ MPa}$ found in the literature overestimated the value of peak scatter (mean values of fundamental and second harmonic response at resonance of 9.8×10^{-3} and $1.8 \times 10^{-3} \text{ Pa}^2 \text{ s}$, respectively, as compared with 1.9×10^{-3} and $3.6 \times 10^{-4} \text{ Pa}^2 \text{ s}$ measured experimentally). A reduced value of $G_s=10 \text{ MPa}$ was found to give improved agreement with the experimental results, as shown in Fig. 2 (this value is dependent on the shell thickness chosen, here $d_s=15 \text{ nm}$). By reducing the value of shell stiffness, although the bubbles become less constrained by the lipid shell (allowing greater relative expansion and contraction), the primary resonance radius is in turn reduced, which also leads to a reduced value of peak scatter. Thus, the calculated mean fundamental and second harmonic responses at primary resonance of 2.9×10^{-3} and $4.5 \times 10^{-4} \text{ Pa}^2 \text{ s}$, respectively, were in excellent agreement to the values measured experimentally. The effect

of changing the value of shell viscosity (η_s) was investigated but found to have a much smaller effect than varying shell stiffness.

The experimental data in Fig. 2 display a variance greater than experimental error calculations predict. Variations of up to 150% in the maximal excursions of optically identical bubbles have been measured previously,^{7,9} attributed to differences in elastic properties of individual shells. The methods presented here allow estimation of such variations from analysis of the acoustic data, and this will be the subject of further work.

Although the Mooney–Rivlin model presented predicts the behavior of Definity® MBs well, discrepancies exist. Asymmetric scatter has been observed here experimentally at resonance, which has been previously suggested to originate in compression dominated behavior induced by buckling of the lipid shell.²⁰ This effect is not described by the Mooney–Rivlin model although other authors have described methods to model this type of behavior.^{9,20} Asymmetric scatter needs to be investigated in the context of subsequent pulse response and will be the subject of further work.

The results of this communication further confirm the robustness of experimentally measured single MB scatter. Indicators which allow the classification of acoustic bubble signals as primary resonant scatter have been identified including increased energy of scatter, increased fundamental to harmonic ratio, and increasing envelope of response with time. This has allowed the acoustic identification of resonant MB scatter for the first time. The techniques presented in this letter provide significant physical insight, and provide the basis for improved signal processing tools for MB imaging.

This work was funded by UK EPSRC Grant No. EP/C523776/1 and British Heart Foundation Grant No. FS/07/052. Support and materials were provided by Lantheus Medical Imaging, N Belarica, MA.

¹V. Sboros, *Adv. Drug Delivery Rev.* **60**, 1117 (2008).

²V. Sboros, S. D. Pye, C. A. MacDonald, J. Gomatam, C. M. Moran, and W. N. McDicken, *Ultrasound Med. Biol.* **31**, 1063 (2005).

³V. Sboros, S. D. Pye, T. A. Anderson, C. M. Moran, and W. N. McDicken, *Appl. Phys. Lett.* **90**, 123902 (2007).

⁴D. H. Thomas, M. B. Butler, T. A. Anderson, R. Steel, S. D. Pye, T. Brock-Fisher, W. N. McDicken, and V. Sboros, *Ultrasound Med. Biol.* **35**, 112 (2009).

⁵L. N. Hand and J. D. Finch, *Analytical Mechanics* (Cambridge, New York, 1998).

⁶A. Jain, M. Murty, and P. Flynn, *ACM Comput. Surv.* **31**, 264 (1999).

⁷M. Posterna, A. Bouakaz, C. T. Chin, and N. de Jong, *IEEE Trans. Ultrason. Ferroelectr. Freq. Control* **50**, 523 (2003).

⁸S. H. Bloch, M. Wan, P. A. Dayton, and K. W. Ferrara, *Appl. Phys. Lett.* **84**, 631 (2004).

⁹M. Emmer, A. van Wamel, D. E. Goertz, and N. de Jong, *Ultrasound Med. Biol.* **33**, 941 (2007).

¹⁰J. B. Keller and M. Miksis, *J. Acoust. Soc. Am.* **68**, 628 (1980).

¹¹A. Prosperetti and A. Lezzi, *J. Fluid Mech.* **168**, 457 (1986).

¹²K. Tsigliffis and N. A. Pelekasis, *J. Acoust. Soc. Am.* **123**, 4059 (2008).

¹³L. Hoff, P. C. Sontum, and J. M. Hovem, *J. Acoust. Soc. Am.* **107**, 2272 (2000).

¹⁴N. de Jong, L. Hoff, T. Skotland, and N. Bom, *Ultrasonics* **30**, 95 (1992).

¹⁵N. de Jong and L. Hoff, *Ultrasonics* **31**, 175 (1993).

¹⁶D. E. Goertz, N. de Jong, and A. F. W. van der Steen, *Ultrasound Med. Biol.* **33**, 1376 (2007).

¹⁷K. Cheung, O. Couture, P. Bevan, P. Burns, and F. Foster, *Proc.-IEEE Ultrason. Symp.* **2**, 850 (2005).

¹⁸K. Vokurka, *Czech. J. Phys., Sect. A* **35**, 28 (1985).

¹⁹D. B. Khismatullin, *J. Acoust. Soc. Am.* **116**, 1463 (2004).

²⁰P. Marmottant, S. van der Meer, M. Emmer, M. Versluis, N. de Jong, S. Hilgenfeldt, and D. Lohse, *J. Acoust. Soc. Am.* **118**, 3499 (2005).